Supersonic helium beam diagnostic for fluctuation measurements of electron temperature and density at the Tokamak TEXTOR

U. Kruezi, H. Stoschus, B. Schweer, G. Sergienko, and U. Samm

Citation: Rev. Sci. Instrum. **83**, 065107 (2012); doi: 10.1063/1.4707150
View online: http://dx.doi.org/10.1063/1.4707150
View Table of Contents: http://rsi.aip.org/resource/1/RSINAK/v83/i6
Published by the American Institute of Physics.

Supersonic helium beam diagnostic for fluctuation measurements of electron temperature and density at the Tokamak TEXTOR

U. Kruezi,[a] H. Stoschus, B. Schweer, G. Sergienko, and U. Samm
Institute of Energy and Climate Research, Plasma Physics, Forschungszentrum Jülich GmbH, Association EURATOM-FZJ, Partner in the Trilateral Euregio Cluster, Jülich, Germany

(Received 28 September 2011; accepted 7 April 2012; published online 14 June 2012)

A supersonic helium beam diagnostic, based on the line-ratio technique for high resolution electron density and temperature measurements in the plasma edge (r/a $>$ 0.9) was designed, built, and optimised at TEXTOR (Torus Experiment for Technology Oriented Research). The supersonic injection system, based on the Campargue skimmer-nozzle concept, was developed and optimised in order to provide both a high neutral helium beam density of $n_0 = 1.5 \times 10^{18}\,\mathrm{m}^{-3}$ and a low beam divergence of $\pm 1^\circ$ simultaneously, achieving a poloidal resolution of $\Delta_{poloidal} = 9\,\mathrm{mm}$. The setup utilises a newly developed dead volume free piezo valve for operation in a high magnetic field environment of up to 2 T with a maximum repetition rate of 80 Hz. Gas injections are realised for a duration of 120 ms at a repetition rate of 2 Hz (duty cycle 1/3). In combination with a high sensitivity detection system, consisting of three 32 multi-channel photomultipliers (PMTs), measurements of edge electron temperature and density with a radial resolution of $\Delta_{radial} = 2\,\mathrm{mm}$ and a maximum temporal resolution of $\Delta t \simeq 2\,\mu\mathrm{s}$ (470 kHz) are possible for the first time. The diagnostic setup at TEXTOR is presented. The newly developed injection system and its theoretical bases are discussed. The applicability of the stationary collisional-radiative model as basis of the line-ratio technique is shown. Finally, an example of a fluctuation analysis demonstrating the unique high temporal and spatial resolution capabilities of this new diagnostic is presented. [http://dx.doi.org/10.1063/1.4707150]

I. INTRODUCTION

In magnetically confined fusion devices the understanding of plasma microturbulence is a key factor to improve their performance. Suitable diagnostics have to be developed to resolve plasma turbulence with sufficiently high temporal and spatial resolution. One possible measurement method is the application of beam emission spectroscopy (BES) on injected thermal helium,[1] also known as line-ratio technique. It utilises an atomic beam which is injected into the plasma edge. The helium atoms interact with the plasma, resulting in the emission of photons. This emission is observed perpendicular to the beam injection. The spatial resolution of this well localised measurement is defined by the cross section of the line of sight with the beam and is typically in the range of a few millimeter.

Thermal lithium beam fluctuation measurements[2] at the midsize Tokamak TEXTOR have been used to characterise radial turbulent transport in the plasma edge. Turbulent structures were observed in the range up to 100 kHz with a spatial size (correlation length) of 3−13 mm (3–4 times larger poloidal correlation length). However, this diagnostic was only capable of studying electron density fluctuations. To characterise the heat transport, electron temperature fluctuation measurements are also required.

Thermal helium beam diagnostics, based on effusive sources, have been established at TEXTOR as standard plasma edge diagnostics to determine both the electron density n_e and temperature T_e profiles simultaneously with time scales of a few milliseconds. These diagnostics cannot be used for turbulence measurements as their beam divergence (typically $\pm 15^\circ$) is too high.

A different type of gas injection system is necessary to provide both a low beam divergence/narrow beam width ($\pm 1^\circ / \Delta_{poloidal} = \Delta_{toroidal} \cong 10\,\mathrm{mm}$) and a high local beam density. The only injection systems able to generate such narrow thermal atomic beams are based on supersonic gas expansions into vacuum and exist in various laboratory experiments. The Tokamak environment with its strong magnetic fields and space restrictions are challenging for the realisation of such beams. Although supersonic injection systems have been realised and used at H-1 heliac[3] and TJ-I UP/TJ-II,[4,5] none of the existing injection systems have been designed to generate beam densities suitable for turbulence measurements.

A new supersonic helium (SHE) beam diagnostic has been developed and brought into operation to investigate short time and spatial scale events in the plasma edge of TEXTOR. It consists of a high performance injection source and an associated fast observation system. The new intense and modulated supersonic injection source is based on the Campargue-nozzle-skimmer scheme. In parallel, a new optimised low noise detection and fast acquisition system was designed and built.

This new helium beam diagnostic and its performance will be presented in this article, which is organised as follows: In Sec. II a brief introduction to the beam emission spectroscopy on helium is presented. To deduce n_e and T_e, a stationary collisional-radiative model (CRM) is used and

[a]Electronic mail: u.kruezi@fz-juelich.de.

the restrictions of the CRM associated with events on short time scales are discussed. In Sec. III the physics related to supersonic gas injections is briefly summarised. In Sec. IV the experimental setup is shown and in Sec. V the experimental results and a short discussion takes place.

II. BES ON THERMAL HELIUM

BES on thermal helium, a line-ratio technique, is an established method to measure the electron density n_e and temperature T_e in the plasma edge of TEXTOR ($2.0 \times 10^{18} < n_e < 2.0 \times 10^{19}\,\mathrm{m}^{-3}$, and $10\,\mathrm{eV} < T_e < 250\,\mathrm{eV}$). The systematic error of the method is $\pm 10\%$ for n_e and $\pm 30\%$ for T_e.[6]

Typically, neutral thermal helium beams are injected into the plasma with the help of effusive sources, because of their simplicity. The plasma parameters are then deduced from the interaction of the beam atoms with the plasma.[1,7–10]

A. Measuring electron density and temperature

A helium atom entering the plasma is first excited from the ground energy state to higher states by electron-electron collisions. The emitted light therefore depends on the local electron density. The depopulation of the higher states depends on either the emission of photons or further electron collisions. Hence, the ratio of light intensities originating from a state which is depopulated mainly by radiation and another state mainly depopulated by electron collisions will be proportional to the local electron density in the plasma. This is the case for the helium line intensities of the singlet system.

The local electron temperature of the plasma has a distinct effect on the singlet and triplet line intensities. The relative population density in the triplet system is reached at lower T_e than those in the singlet system due to the particular dependence of the rate coefficients on the temperature.

This dependence of helium line intensity ratios on both n_e and T_e can be used to determine these plasma parameters themselves by comparing measured emission profiles with calculated profiles based on a CRM.

In particular, the ratios of the line emission profiles of the following wavelengths $\lambda_{3^1D\rightarrow 2^1P} = 667.8$ nm, $\lambda_{3^1S\rightarrow 2^1P} = 728.1$ nm, and $\lambda_{3^3S\rightarrow 2^3P} = 706.6$ nm ($R_{n_e} = 667.8/728.1$ and $R_{T_e} = 728.1/706.5$) are used, where the first ratio is mainly dependent on n_e and the second on T_e.

To simplify this analysis procedure, a stationary method is standardly used at TEXTOR assuming all involved atomic states being in equilibrium.

B. Influence of the relaxation time

As a consequence, this method is only valid for signals which stay constant in the timescale of the relaxation time for $n_e \cdot (dn_e/dt)^{-1} \approx \tau$ or $T_e \cdot (dT_e/dt)^{-1} \approx \tau$. As the typical relaxation times for the singlet states are one order below the times of the triplet states, the latter defines the time constants for the used method. In Figure 1, the relaxation time of the meta-stable triplet state 2^3S is shown as a function of n_e and T_e.[8] A strong dependence of the relaxation time on T_e for $T_e < 20\,\mathrm{eV}$ can be seen, whereas for $T_e > 20\,\mathrm{eV}$ only a dependence on n_e can be found. In general τ decreases with n_e. An application of the stationary method on line intensities originating from non relaxed states leads to an overestimation of the temperature. As a consequence, the atoms passing the observation volume lead to a smearing along their path. In Figure 2, this effect is illustrated in the frame of the observation volume given by the fixed detector size Δr_D. The atoms passing the observation volume with their initial velocity v require a certain volume Δr_τ for a complete relaxation. For a typically low density at TEXTOR of $2 \cdot 10^{18}\,\mathrm{m}^{-3}$($\tau = 2.512 \times 10^{-6}\,\mathrm{s}$) and a beam velocity of $v = 1760\,\mathrm{m/s}$, this volume is approximately $r_\tau \simeq 4.4$ mm. With the increasing density towards the plasma centre the relaxation time and related volume decreases below the detector resolution. This effect needs to be taken into account when signals are observed in the presence of low plasma densities.

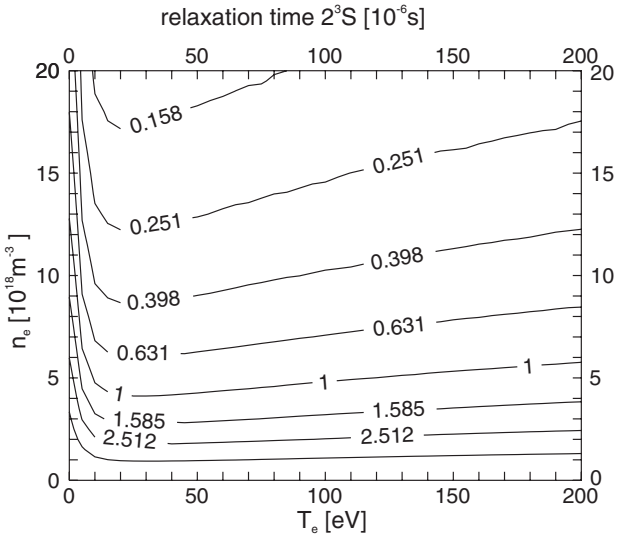

FIG. 1. Contour lines of constant relaxation times in microseconds in the n_e-T_e-plane for the 2^3S triplet system.[8]

C. Signal intensity

For low light level and high bandwidth applications the basic noise, which defines the signal quality, is the photon

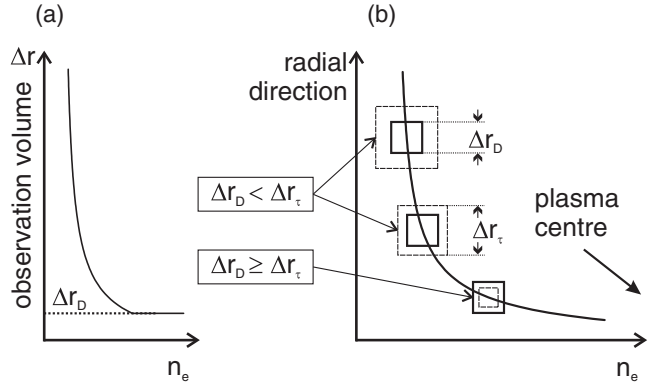

FIG. 2. (a) Minimum resolution based on a fixed detector size Δr_D and the locally smeared observation volume Δr_τ due to the relaxation effect of helium atoms entering the plasma. (b) Size of the effective observation volume Δr for a given detector size.

statistical noise. The noise σ of measured signals, defined by the bandwidth $(1/t_B)$ of the detector electronics and the incoming photon flux $\dot{N}_{Phot}$ obeys the Poisson statistics $\sigma = \sqrt{\dot{N}_{Phot} \cdot t_B}$. Also, this noise increases with higher photon flux and the signal-to-noise-ratio (SNR) improves with $1/\sqrt{N_{Phot}}$. The achievable resolution of fluctuations is primarily determined by the SNR. Therefore, to characterise the efficiency of the diagnostic, a prediction of the expected signal is essential.

The photon flux per steradian, which is emitted by the helium beam atoms, can be calculated as follows:

$$\dot{N}_{Phot} = \frac{1}{4\pi} n_0 \, V \, I_{Phot}(n_e, T_e), \tag{1}$$

where n_0 is the particle density, V is the volume, and $I_{Phot}(n_e, T_e)$ is the emitted photon number per atom/second. The latter depends on the plasma parameters as described above. To estimate a measured signal, optical, and electrical constraints have to be taken into account. The incoming photons are converted into electrical signals, respectively, photo electrons N_{El}:

$$\dot{N}_{El} = \frac{1}{4\pi} \Omega \, T \, \eta \, V \, n_0 \, I_{Phot}(n_e, T_e), \tag{2}$$

where Ω denotes the spatial angle, T is the effective transmission coefficient of the optical components, and η is the quantum efficiency of the detector. In relation to this experimental setup, the following values are given: $\Omega = 1.2 \times 10^{-2}$ sr, $T = 0.17$, $\eta = 0.06$, $V = 2 \times 10^{-7}$ m^3, $n_0 = 1.5 \times 10^{18}$ m^{-3}, and $I_{Phot}(n_e = 6 \times 10^{18}\,\mathrm{m}^{-3}, T_e = 45\,\mathrm{eV}) = 130$ photons/s (taken for the weakest line intensity $\lambda_{3^1S \to 2^1P} = 728.1$ nm). The result for the photo electron flux of 1.9×10^8 s^{-1} indicates a relative noise level for signals in time scales of $\Delta t = 1 \times 10^{-5}$ s of approximately 2%, which is sufficient to measure plasma parameter fluctuations in this frequency range.[11,12]

Significant improvements of the optical and detection systems can not be achieved due to technical limitations. The beam density was the key factor for the optimisation of this diagnostic.

III. REALISATION OF A NARROW HELIUM BEAM

The basic principle to realise a gas injection system is the increase of static pressure in a reservoir and allowing the gas to leave via an expansion process through an orifice or nozzle. The gas flow through this orifice can be described by the Knudsen-number, which is defined as $K = \bar{l}/d$, with the mean free path length $\bar{l}$ and the diameter of the characteristic orifice d, e.g., the diameter of the tube which the gas is passing. Large values of the Knudsen number $K \geq 1$ indicate an unperturbed beam evolution. The properties, e.g., velocity distribution of these regular used effusive injection systems, are well defined by the gas temperature in the reservoir. When taking a closer look at the particle flux of these particular beams, $I \sim p_0 \cdot d^2 \sim d/K_0$ shows that a rise in beam density by increasing the pressure p_0 (index 0 indicates reservoir conditions) in the reservoir will lead to $K < 1$ and a perturbed beam flow. In this case, with increasing stagnation pressure, impacts between the gas atoms will occur and the Knudsen expansion will become a supersonic expansion. The flow properties can then be described by the Mach number $M = \overline{v}/c_S$ which equals one and higher in a supersonic flow. This number is given by the ratio of the mean beam velocity $\overline{v}$ and the sound speed c_S, which itself depends on the local temperature $c_S \sim \sqrt{T}$. The latter decreases as adiabatically expanding gas experiences cooling. The supersonic conditions are fulfilled if the pressure p_0 of a gas, which expands through a nozzle, reaches a critical value with respect to the ambient pressure p_b. This is defined by basic gas dynamics $(p_b/p_0)_{crit.} = (2/(\gamma + 1))^{\gamma/(\gamma - 1)}$ with the adiabatic constant γ.[13–15] This means that a supersonic expansion of an ideal gas ($\gamma = 5/3$ for helium, $p_b/p_0 = 0.49$) evolves already if the reservoir pressure is 2 times higher than the ambient pressure. The mean velocity of the helium beam, which is defined by the energy conservation law, is slightly increased to $\overline{v}_{max} = 1760$ m/s ($T_0 = 300$ K) compared to the thermal velocity $v_{th} = 1260$ m/s in the reservoir. A more distinguished change appears on the beam divergence, as the beam atoms stop to suffer impacts with decreasing temperature and become monoenergetic. In this case, their diverging trajectories originating from the nozzle are becoming straight lines and no additional thermal spread appears.[16]

This property of supersonic beam injections is a main precondition to generate narrow beams.

In technically realisable vacuum systems with restricted pumping efficiency, the background pressure will start to increase with the injection of gas reaching an equilibrium state between the pumping capacity and the injected amount of gas. The beam atoms leaving the nozzle will suffer impacts with these background gas atoms and a Mach cell structure will be created, schematically shown in Figure 3. The inner part of this cell is called "Zone of Silence," inspired by a strong decrease in sound speed (high values of the Mach number) within this area, where principally no perturbation or shock wave can propagate. Downstream, the Mach cell structure ends at the "Mach plane," which is placed at a distance x_M

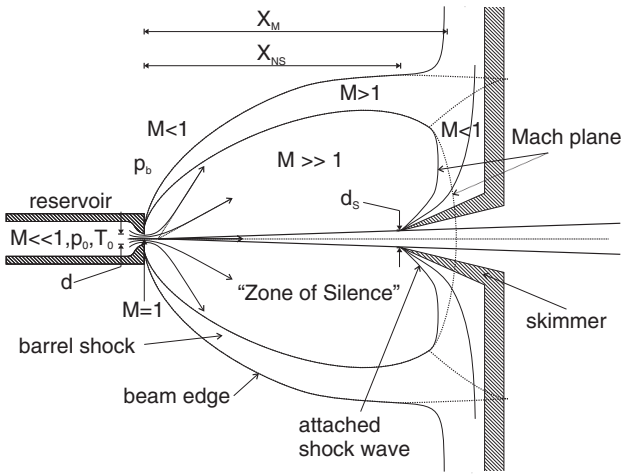

FIG. 3. Scheme of mach cell structure. The Mach plane is placed downstream of the nozzle and terminates the supersonic flow (dotted lines). The insertion of a skimmer changes the shape of the Mach cell structure (solid lines) and an attached (shown case) or detached ("bow shock") shock wave appears at the skimmer tip or in front, respectively.[17]

in front of the nozzle[18]

$$\left(\frac{x_M}{d}\right) = 0.67\sqrt{\frac{p_0}{p_b}}\,. \tag{3}$$

Beam atoms reaching this area or passing it will immediately become thermalised and will lose their supersonic properties. This restricts the use of this kind of beam to the extent given by Eq. (3).

To overcome this problem, Campargue[19,20] suggested the insertion of a material skimmer into the "Zone of Silence." Although this was not the first time a skimmer has been proposed to produce a supersonic beam, his approach was based on the fact that the background gas cannot penetrate in the higher density region of the "Zone of Silence." With this method it is possible to transfer the Knudsen number from the nozzle $K_0 \ll 1$ to the skimmer opening $K_S = 1$ (Knudsen number at the skimmer) and to fulfil the Knudsen condition.

A. Campargue-type supersonic injection system

Nevertheless, a very accurately made skimmer with special shape, dimensions, and precise positioning in the beam centre, is the main problem in achieving this setup. The insertion of a skimmer leads to a deformation of the mach cell which can be seen in Figure 3. Shock waves originating from interactions between the skimmer and the gas atoms can evolve and take position close to the beam centre or as a "bow shock" in front of the skimmer. This would strongly interfere with the beam and reduce its intensity.

Under almost perfect conditions ambient pressures in the range of a few millibar would be acceptable if the reservoir pressure is high enough and the skimmer opening and leading edge is adjusted to these conditions. At first sight, this appears to be contrary to the idea of the mean free path which should be at $\bar{l} = K \cdot d = 1/(5.3 \cdot p) = 0.189$ mm[14] for helium at this ambient pressure. But the penetration of the ambient gas is strictly suppressed by the high local density in the "Zone of Silence," which shields the undisturbed core of the beam with its "local effective mean free path." The nozzle skimmer distance x_{NS} has to be chosen very carefully to minimise the perturbation effects appearing in the "Zone of Silence" between the skimmer and the beam atoms. By moving the skimmer too close to the nozzle, a higher density will lead to a stronger interference and a decrease in the effective beam intensity and an increase in the divergence $I \sim \exp(K_S^{-1}) \sim \exp(x_{NS}^{-14/9})$.[21] Positioning the skimmer too far from the nozzle could bring it close to the Mach plane and penetrating background gas atoms could reduce the intensity according to Beer's law $I \sim \exp(-\,p_b \cdot x_{NS})$ (approximation for low background pressures). This implies that an optimum position must exist. This position is generally placed at $0.6 - 0.7 \cdot x_M$[20] where the "belly" of the Mach cell structure can be found.[22] Although these parameters show how to design an optimised injection system, the real setup will usually be defined by the boundary conditions in the experiment, e.g., the required beam width for available skimmer diameters which primarily will define the setup. The divergence, and therefore the beam width at a certain position downstream, can be calculated approximately by the simple theorem on intersecting lines. The beam stream lines are originating from a central point at the nozzle plane (for circular nozzles)[18] and diverging in straight lines from this point. Hence, the beam flux density[14] can be calculated by

$$\Phi = \frac{I_0\Omega}{A_p} = \frac{\kappa\Omega}{\pi A_p}\frac{dN}{dt} \tag{4}$$

with κ as the peaking factor, which describes the source efficiency in comparison to an effusive source. In general, it is constant ($\kappa = 2$) for supersonic injection systems. The solid angle $\Omega = \pi/4 \cdot (d_S/x_{DS})^2 = A_S/x_{DS}^2$ with the skimmer opening surface A_S, the beam cross section in the observation volume $A_p = \pi/4 \cdot \Delta_p^2$, given by the poloidal beam width of $\Delta_p = 10$ mm (circular beam), and the helium flux at a gas temperature of $T_0 = 300$ K by

$$\frac{dN}{dt} = 1.09 \times 10^{19} p_0 \cdot d^2 \text{ mbar}^{-1} \text{ mm}^{-2} \text{ s}^{-1} \tag{5}$$

finally define the beam flux density Φ.

Equation (4) depicts that the well known high intensity of supersonic beams results not from their beam flow properties ($\kappa = const.$), but by the choice of higher particle fluxes dN/dt. These could be increased based on the efficiency of the vacuum system, providing a sufficiently low pressure in the nozzle skimmer chamber.

IV. EXPERIMENTAL SETUP

On this theoretical basis, we have developed a new diagnostic and characterised it in the laboratory.[8,23] Finally, it has been installed and brought into operation at the fusion experiment TEXTOR.[24] This experiment is based on a high temperature plasma, which is magnetically confined in the Tokamak configuration. TEXTOR is a midsize Tokamak with plasma pulses of up to 10 s length at a toroidal magnetic flux density of $B_t = 2.8$ T on the axis and a typical plasma current of $I_p = 500$ kA. The small radius is at $a = 0.46$ m and the large radius at $R = 1.75$ m.

The newly integrated supersonic helium beam injection system is installed on top of the toroidal vacuum chamber and injects the gas vertically into the plasma (see Figure 4(a)). It consists of the following basic elements:

1. The Campargue-type nozzle skimmer system with a newly developed piezo valve to generate a modulated beam through a micro nozzle and a skimmer. The modulation of the beam effectively reduces the requirements of the vacuum system with respect to a steady state injection. Additionally, it provides an efficient way of background subtraction during plasma operation.
2. A vacuum insertion enabling the beam source to be moved into the main TEXTOR vacuum vessel. This reduces the distance between the beam source and the observation volume and is used to raise the beam density by increasing the divergence but maintaining a low beam width in the observation volume.
3. A powerful vacuum pumping system to remove the background gas. Using volume pumping of this chamber and changing the duty cycle of the modulated beam source enables higher beam fluxes.

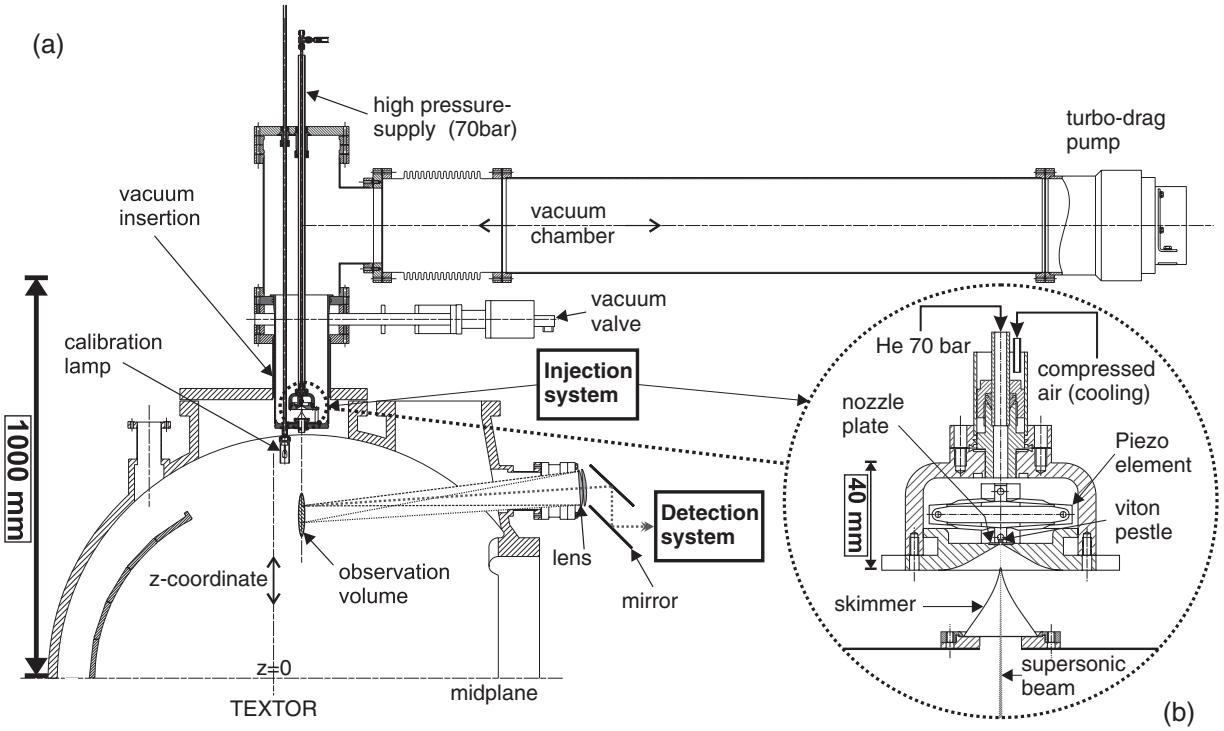

FIG. 4. (a) Overview of the supersonic injection system mounted at the Tokamak TEXTOR. The holding structure of the injection system and toroidal field coils are not shown. (b) The new piezo valve and the actual nozzle-skimmer injection system.

The associated detection system (see Figure 6) has been built up to follow alternating optical signals up to a few hundred kilohertz.

The beam emission is observed perpendicular to the injected beam. Two observation sub-systems which work in parallel can be specified:

1. The camera system. It has been designed to provide both the basic beam properties, such as intensity or beam width (2D), and to enable a relative calibration procedure of the second sub-system.
2. The photomultiplier (PMT) system (1D array). In particular this is used to achieve a high time resolution.

Both sub-systems are equipped with an appropriate data acquisition. Additionally a control system provides the synchronisation with the plasma pulse, the gas injections, and the differing sample frequencies of the detector sub-systems.

A. Injection system

On the basis of the theoretical background in Sec. III and the constraints at the TEXTOR environment, we have designed an injection system, which will be described in the following.

1. Piezo valve and nozzle-skimmer system

The newly developed modulated valve, which can be seen closer in Figure 4(b), provides an operation in high magnetic field environments and has been tested up to 2.6 T. The gas is located in a high pressure reservoir, which provides a continuous and stable gas flow through the diverging central nozzle plate (*Metaq*, nozzle diameter $d = 40 \pm 2\,\mu$m, exit plane diameter $120\,\mu$m, plate thickness $100\,\mu$m - optically determined). It is attached to the bottom part of the vessel, which has an opening angle of 120°. The nozzle plate can be replaced if required by available plates with various diameters (10–70 μm). Inside the high pressure vessel, which can be loaded with pressures up to 100 bar, a piezo element (*Piezosystem, PX 500*) is mounted. One end of the axis is equipped with a viton pestle and the opposite side is mounted and fixed in place. The application of a voltage at the piezo element results in an expansion of about $500\,\mu$m which removes the pestle from the orifice at the nozzle high pressure side. In this configuration the piezo element acts as a valve. In combination with the diverging nozzle plate, it is working virtually dead volume free with a maximum repetition rate of approximately 80 Hz and is insensitive to magnetic fields. The repetition rate in the present system can be chosen in steps of 1 ms, increasing up to 1 s with independent sets of open and close cycle times. For a reliable operation, the temperature of the piezo element should be kept below 70 °C, which has been realised with sufficiently precooled injection gas. A robust solution has been found by the application of a coaxial cooling of the injection gas supply line using compressed air (see Figure 4(b)).

To achieve the required beam divergence in the observation volume, a skimmer (*Beam Dynamics*, $d_S = 210\,\mu$m, leading edge of 5 μm thickness) is placed at an adjustable distance in front of the nozzle and the high pressure vessel.

2. Vacuum insertion

To increase the beam density inside the observation volume an additional measure has been applied. By using a

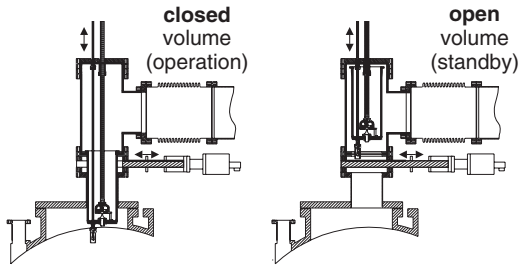

FIG. 5. The vacuum insertion concept to reduce the distance to the observation volume. The bold black lines indicate the open and close chamber.

vacuum insertion to reduce the distance between the skimmer opening and the observation volume to 270 mm, the divergence of the beam and the beam density could be increased significantly, whereas the beam width in the observation volume could remain at a low value (∼10 mm). With the present setup, the entire nozzle-skimmer system, including the valve, is fixed on a unique open topped vessel and can be inserted by a linear displacement unit, and a handwheel without breaking the TEXTOR vacuum inside the main vacuum chamber of the Tokamak. Only in its final position is the injection system operational (presented in Figure 4(a)) and can provide a closed and separate vacuum chamber. The functional principle of the vacuum insertion is illustrated in Figure 5. With this moving vessel, it is possible to separate the diagnostic vacuum system for maintenance reasons (standby) from the TEXTOR vacuum. During operation in the inserted state, only the skimmer opening connects both systems.

Close to the valve, a movable calibration lamp is installed to adjust the detectors to the observation system. It can be moved manually to the centre line of sight inside the TEXTOR vacuum chamber.

3. Vacuum pump system

The nozzle-skimmer setup has been designed to be as compact as possible in order to reduce the conductance value of the streaming gas inside the vacuum insertion. The effective pumping efficiency S_{TP}^{eff} varies with the background pressure in the vacuum vessel and is approximately 40%–60% of the nominal value of the turbo pump.

The large branch connection in Figure 4 is connected to a turbo drag pump TMU 1600 (*Pfeiffer*, $S_{TP}^{nominal} = 1450$ l/s for helium) via a long vacuum tube (diameter of 250 mm). The pump must be placed far enough from the magnetic field coils (not shown in Figure 4) to avoid eddy currents in the rotor blades of the pump, which could cause damage. A powerful rotary pump Trivac D65B (*Leybold*, $S_{RP} = 18$ l/s for helium) removes the gas pumped by the turbo drag pump, whose operational pressure should not continuously exceed $p_{pv} = 5$ mbar at its exit. This restricts the maximum tolerable background pressure in the vacuum chamber, which can be deduced from the continuum equation $p_{pv} \cdot S_{RP} = p_b \cdot S_{TP}$, and in this case is $p_b^{max} = 1.5 \times 10^{-1}$ mbar ($S_{TP}^{eff} = 0.4 \cdot S_{TP}^{nominal}$, $S_{RP}^{eff} = S_{RP}^{nominal}$).

The pressure in the vacuum chamber is monitored by a set of absolute pressure Baratron gauges (*MKS*) and Ionivac (*Leybold*) pressure gauges. The complete vacuum system can be controlled remotely by pressure valves connected to a Simatic S5 (*Siemens*) control unit.

To increase the amount of injected gas, other than by the measures mentioned above, the large vacuum chamber of the present system itself is used as a pump with practically infinite pumping efficiency using the "volume pumping effect." This means that the chosen gas flow into the chamber can be much higher than would be acceptable for a steady state beam flow. By stoping the injection at the critical background pressure p_b^{max}, the system could be held operational. The vacuum system is then reducing the gas pressure down to a certain value before the next gas injection.

Due to the restricted pumping speed and the available volume of the present vacuum chamber, the suitable working duty cycle of 1/3 is given by a modulation of 120 ms for the injection and a pumping period of about 380 ms (2 Hz effective repetition rate).

With respect to the time scale of the desirable observation of the plasma fluctuations, these modulation parameters (120 ms $\gg$ 10 μs) do not restrict the measurement, therefore the injection system can be treated as a quasi stationary.

B. The detection system

In addition to the new injection system, a detection system has been developed and optimised to measure signals with high temporal resolution to fulfil the requirements for the signal intensity introduced in Sec. II. This detection system is shown in Figure 6 from top view. The beam emission is observed perpendicular to the injected beam through a vacuum window and is projected to the detectors with the help of an optical setup (lenses, mirrors, beam splitters). The observation system consists of two sub-systems which work in parallel, the camera system, and the PMT-system. Whilst the camera provides data on a longer time scale (∼ms), the PMT-system observes signals on a shorter time scale (∼μs). To eliminate typical problems of photomultipliers, such as signal drifts or different spectral and gain dependent differences of devices, a relative calibration procedure between the camera and the PMT system can be applied simultaneously during measurements.

For this calibration, the 2D camera signal is extracted corresponding to each PMT-cathode area. The PMT signal is then integrated according to the time resolution of the slower camera system. Finally, the signal is normalised to the camera signal.

The adjustment of both sub-systems to one identical reference point can be achieved with the help of the calibration lamp shown in Figure 4.

The entire injection and observation system has been designed and installed in consideration of accurate grounding (e.g., avoiding grounding loops) and shielding schemes for the detectors, the data acquisition, and the control system to reduce broadband noise.

1. The camera observation system

The light signal originating from the interaction between helium beam and plasma is observed in parallel by both

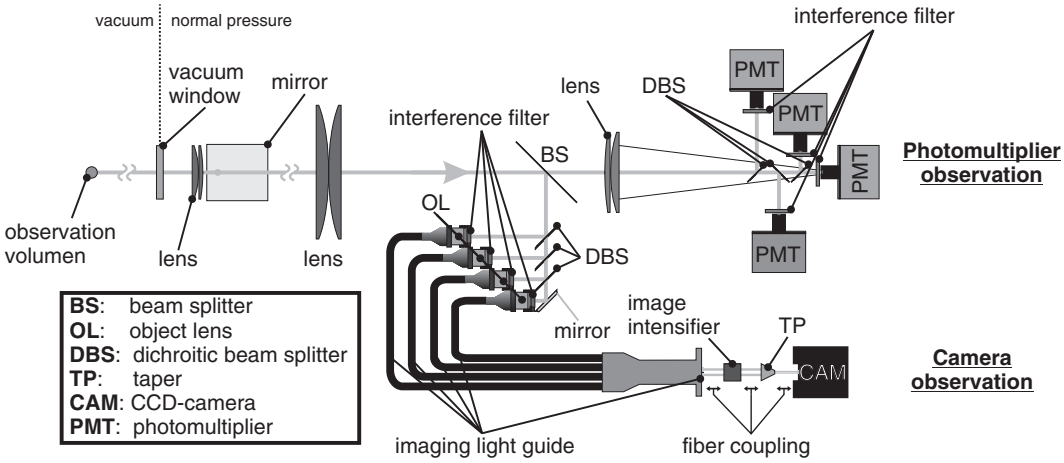

FIG. 6. Schematic view of the detection system from top view.

sub-systems and is divided by a beam splitter (Reflection 20%, Transmission 80%). An array of dichroitic mirrors preselect the wavelength ranges for the three requested wavelengths and a fourth wavelength for a free additional purpose. The actual wavelength is then chosen by narrow interference filters (*Andover*, FWHM 1.5 nm). In the camera system these filters are placed directly in front of object lenses (*Schneider-Kreuznach*, Xenoplan 1.9/35 mm) which couple the light into an imaging light guide bundle (*Schott*, SK-8399). This light guide consists of four single light guides ($4 \times 4\,\text{mm}^2$), which are merged at the exit to one 2×2 matrix ($8 \times 8\,\text{mm}^2$). This fibre exit is connected to an image intensifier (*Proxitronic*, S20 cathode) with a fiber coupling entrance. The actual camera (*Dalsa*, 256×256 pixel) is connected to the phosphor anode of the image intensifier via a 2:1 taper.

This setup enables the measurement of four equal but spectrally separated images with one camera and one image intensifier. The minimum spatial resolution of 1.1 mm is defined by the imaging light guide resolution.

2. The photomultiplier observation system

The photomultiplier observation has a comparable setup with dichroitic mirrors and interference filters. The multianode photomultipliers H7260-20 (*Hamamatsu*, 32 channel $-0.8 \times 7\,\text{mm}^2$) with linearly oriented channels of 1 mm distance to each other and a low crosstalk (<1%) with a quantum efficiency of 6%, are placed in the image plane directly behind the interference filters. In this case, the higher incident angle leads to a 2D transmission curve for the interference filters, and therefore a strong distortion of the image light intensity (e.g., effectively 38% below the maximum of the IF transmission for a 0° incidence angle at $\lambda = 728.1\,\text{nm}$) appears. The camera system (with a distortion <1%) is used to correct this distortion.

The spatial resolution of the photomultiplier system is defined by the magnification for the optical system (m = 0.5) and the cathode size of the PMT, which results in a resolution of 32×2 mm in radial and a light integration of 14 mm in toroidal direction. The effective transmission of this optical setup is about 17% (assuming a transmission loss of 4% per optical surface) and about 10% for the camera system, including the light amplification of the image intensifier into the transmission.

3. The acquisition electronics

The entire electronics of the PMT system has been developed and manufactured to achieve a 470 kHz bandwidth, digitally sampled at 800 kHz. The electronics consists of surface mounted device (SMD) technology based current to voltage converter platines (schematically shown in Figure 7) with a bandwidth of 800 kHz and an output voltage of about 0.05–3 V (max. $3\,\mu\text{A}$). To achieve a high bandwidth and to reduce the noise, it is necessary to minimise the parasitic capacitance C_p. This is achieved by a design geometry which provides the shortest possible connection distance between the PMT anode output and operational amplifier input. The converters are directly plugged to the anode output of the 32 channels ordered in a 2×16 connector array at the rear

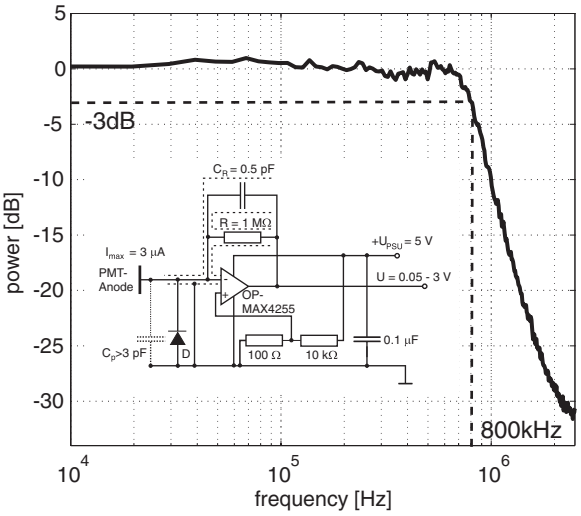

FIG. 7. Frequency behavior and electrical scheme of the current to voltage converter manufactured in SMD technology (frequency resolution: $\Delta f = 10\,\text{kHz}$). The overall bandwidth is restricted to 470 kHz at the line driver output with the help of a low pass filter.

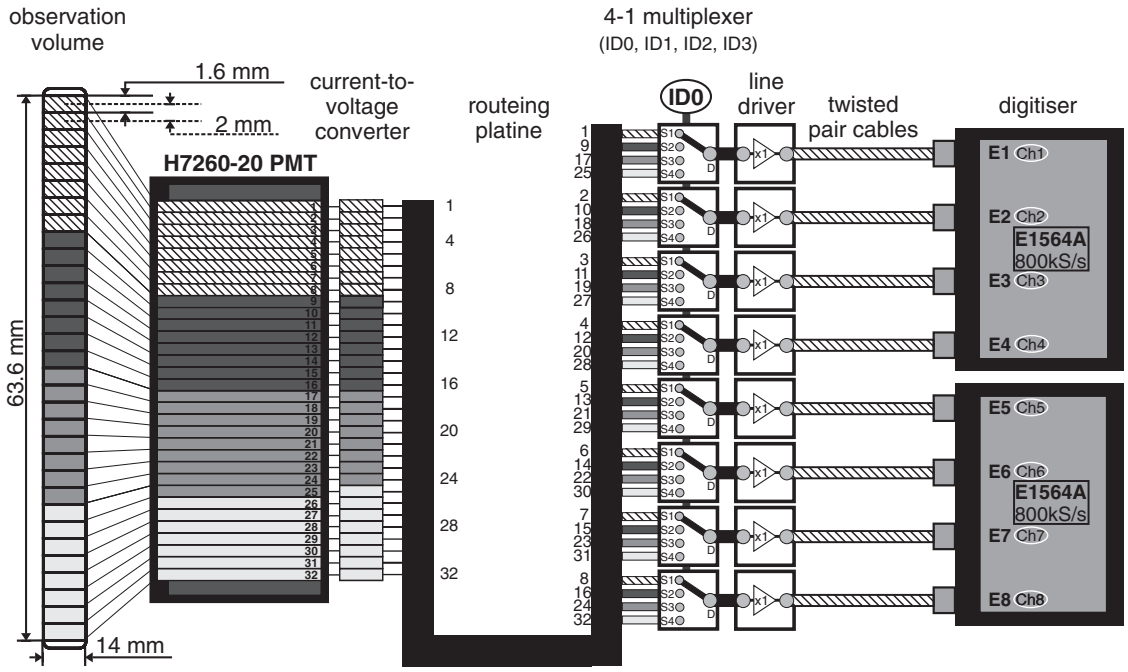

FIG. 8. Schematic of the acquisition electronic of one multichannel PMT H7260-20 with the connected current to voltage converter electronics, the routeing platine, the multiplexer array, and the VXI data acquisition modules. The multiplexer position is controlled by the particular ID applied to it (ID0 is shown).

side of the PMT (distance between neighboring connectors 2.54 mm).

As only 8 channels of the 32 can be acquired simultaneously with the existing data acquisition, a further advantage has been taken of the miniaturised electronics. The converted voltage does not enter the data acquisition directly but is fed into a multiplexer board of eight 4:1 multiplexers to reduce the output channels from 32 to 8 (schematically presented in Figure 8). This multiplexer can be switched and feeds the 8 acquisition channels with various PMT channel outputs. For additional flexibility, the connected signals can be rerouted on a dedicated platine before entering the multiplexer board. Various wiring combinations, with different routeing platines, can be chosen for each measuring task. To scan the whole radius a routing platine is standardly connected, which enables a sweep of 8 observation channels (in the mode: 1–8, 9–16, 17–24, 25–32, controlled by the multiplexer ID: 0, 1, 2, or 3, respectively) in between gas pulses. The last stage of this detection electronic consists of signal filters and line drivers. Their purpose is to minimise the aliasing effect by restricting the bandwidth to approximately 470 kHz, and to provide a stable output signal over a cable length of 15 m to the data acquisition hardware.

4. Data acquisition and control

A data acquisition and control system has been developed to fulfill the experimental requirements of the SHE diagnostic.

For the data acquisition, a combination of CAMAC and VXI-digitisers is used. The CCD-camera data is acquired by one VXI 1ch-100MHz digitiser with external trigger and sample clock input. Six 4ch-800kHz differential input digitisers provide the data acquisition for three PMTs, hence signals on eight spatial channels per PMT can be acquired simultaneously. The CAMAC digitisers are generally used for slower signals, such as gas pressure or SHE status signals. All digitiser modules are equipped with local memory modules. The data transfer from these local digitiser modules to the final data storage is done in between plasma pulses.

The control of the data acquisition is performed by a stand alone hardware, which has been designed to generate all characteristic digital signals necessary to reconstruct and acquire the measured signals with the high temporal accuracy. For this purpose, the control system is internally running on one single master clock frequency of 16 MHz. This clock frequency is used to run the CCD-camera system and its signal acquisition. The camera frame rates (50–200 Hz) can be changed manually at the integrated camera control interface.

Furthermore, the master clock is used to generate the sample frequency of the multichannel PMT data acquisition at 800 kHz. To achieve a synchronisation this sample clock is generated with the help of internal frequency dividers, which reduce the 16 MHz master clock to the required frequency. Synchronisation is crucial if recorded events are to be compared with results of other diagnostics.

The multiplexer system shown in Figure 8 is controlled in a similar way and can either be switched between gas injections from one observation volume to another, which enables the acquisition of data over a full profile during one plasma pulse, or stays fixed at one observation position.

The modulated gas injection (1–1000 ms) timing is provided, based on the same frequency divider technique. The active gas injection is the main criterium for the data acquisition and can be changed on the beam timing module in steps of 1 ms with separated beam on and off phases.

With this structure, a synchronisation of 1/16 MHz can be assured for the whole SHE diagnostic. Various BNC/LEMO

inputs and outputs can be used to monitor and acquire control signals such as the frame synchronisation.

V. RESULTS AND DISCUSSION

The new supersonic helium beam diagnostic has been developed to investigate plasma fluctuation in the plasma edge of TEXTOR. For this purpose, the beam width and the particle flux have been optimised and an optical observation with a high throughput has been designed and brought into operation.

In the following, a brief characterisation of the injection system is presented with respect to divergence and particle flux of the installed and operational system at TEXTOR. This is followed by first measurement results of the completed diagnostic presenting possible measurement ranges and capabilities as a proof of principle.

A. Helium beam width

In Figure 9(a) the toroidal beam profile created by different reservoir pressures during a standard plasma pulse is shown based on the emission profile of the $\lambda = 728.1$ nm helium line. This profile has been taken at the central observation position ($z = 470$ mm) at a distance $x_{NO} = 270$ mm from the nozzle. It can be seen that the profile has a Gaussian shape which has already been observed with the help of Pitot probe measurements in the laboratory with $x_{NO} = 440$ mm and $x_{NS} = 9$ mm shown in Figure 9(b). Therefore, there is no need for the profile to be Abel transformed and it can be interpreted directly due to its invariant properties of the Gauss curve. The beam width does not stay fixed and has a tendency to increase with increasing reservoir pressure. This has also been observed in the laboratory. The nozzle skimmer distance of $x_{NS} = 10$ mm would theoretically result in a beam width of $\Delta_p = 5.7$ mm but is about 60% higher in the shown 70 bar pressure case. In laboratory measurements this broadening was specified with less than 30%. The increasing beam width is mainly a result of the interaction between the beam particles and the skimmer which leads to a decrease in beam intensity, as explained above, and additionally to an influence on the beam shape. The latter is particulary detrimental if a displacement of the skimmer from the beam axis occurs. While the beam axis could have been adjusted in the laboratory, this is not possible for the setup at TEXTOR. It is simple to calculate that a relatively small displacement of the skimmer in the range of 0.3 mm would result in a shift in the beam axis of 8 mm within the observation volume. This shift has been observed during plasma pulses and an influence on the beam shape, for example, on the beam width, has to be expected. However, this is not a restriction for measurements, but rather leaves space for future optimisation.

B. Helium beam particle flux

The gas injection leads to a pressure increase in the vacuum system. This pressure increase can be used to deduce the particle flux applying the ideal gas law based relation

$$\frac{dp_b}{dt} \cdot V = \frac{dN}{dt} \cdot k_B \cdot T - S \cdot p_b,$$

with the Boltzman constant k_B, the Temperature T, and the vacuum chamber volume V. As the background pressure in the vacuum chamber can reach values up to $p_b = 1.5 \times 10^{-1}$ mbar, it is becoming difficult to deduce the pumping efficiency from the exponential decay $p_b = \exp(-\frac{S}{V}t)$, which is a usual method for vacuum systems with modulated gas injections. This method can not be applied if the pumping efficiency varies with the background pressure, which is the case for the used turbo molecular pump and the appearing pressure range. In this case, a dynamic method to determine the pumping efficiency depending on the background pressure must be used, based on $S(p_b) = \frac{d}{dt}(-V \cdot \ln(p_b))$. The pumping efficiency is extracted for each background pressure level instead

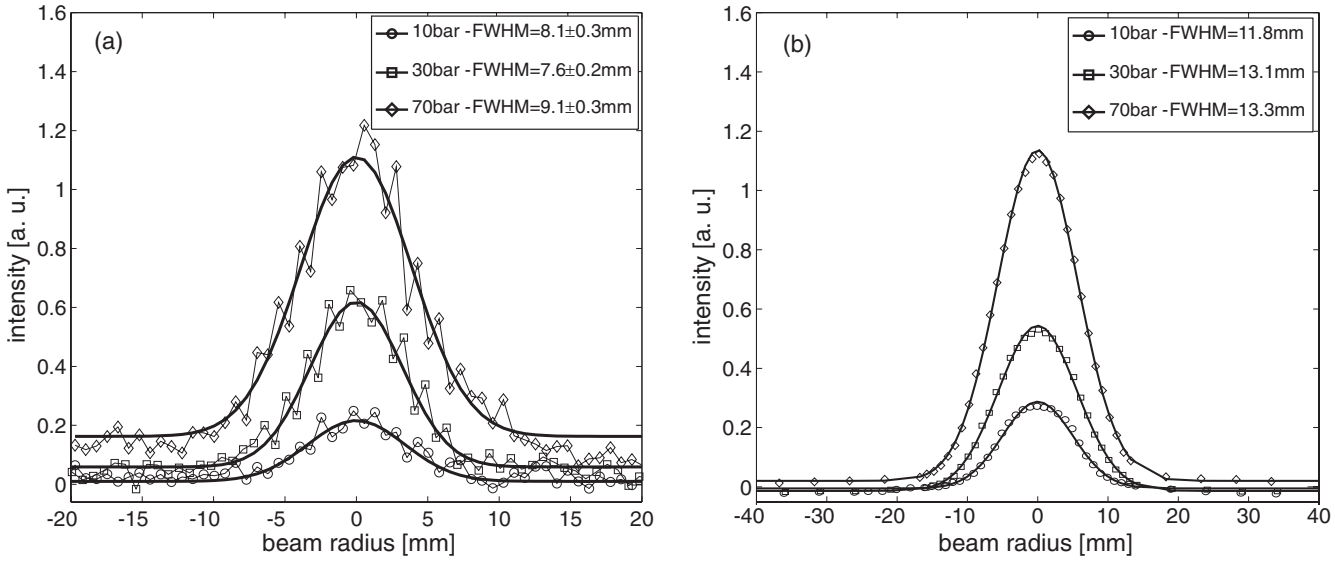

FIG. 9. Toroidal profiles measured during a standard discharge spectroscopically on the emission profile of $\lambda = 728.1$ nm. (a) In TEXTOR at a distance $x_{NO} = 270$ mm downstream the nozzle, and (b) in the laboratory measured with a Pitot probe at $x_{NO} = 440$ mm.

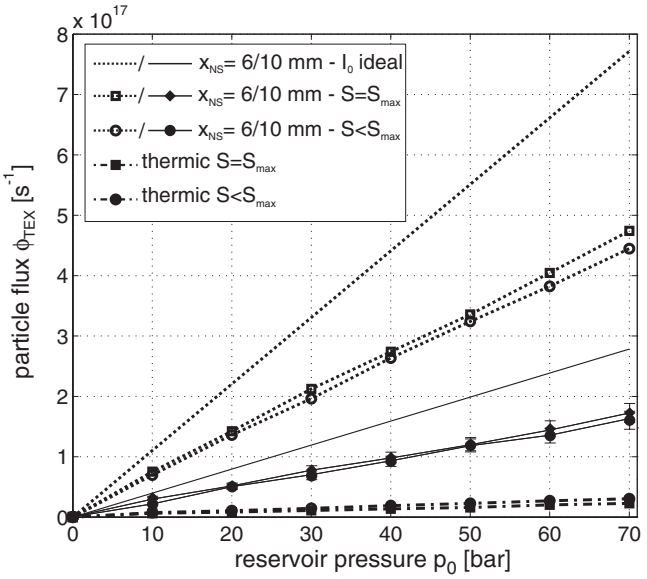

FIG. 10. Particle flux with and without a free supersonic beam evolution for two nozzle-skimmer distances ($x_{NS} = 6$ mm dotted lines and $x_{NS} = 10$ mm solid line). The thermic case has been generated by blocking the direct path of the beam between nozzle and skimmer.

of using one constant pumping efficiency. Using this method, the measured background pressure can be transferred to a particle flux depending on the reservoir pressure. A linear fit of this curve leads to a particle flux

$$\frac{dN}{dt} = 1.81 \times 10^{19} \cdot p_0 + 7.88 \times 10^{18}\ [\mathrm{bar}^{-1}\ \mathrm{s}^{-1}].$$

The second term can be seen as the error of the method and can be neglected for high reservoir pressures. A comparison with Eq. (5) can be used to recalculate the effective nozzle diameter. The result is a diameter of $d = 41\,\mu$m which is within the error bar for the optical determination and proves the above method to be right.

Only a small portion of this particle flux will enter the TEXTOR vacuum chamber through the skimmer orifice. This particle flux ϕ_{TEX} can bee seen in Figure 10 for two different nozzle skimmer distances. The same method as above was applied to achieve the particle flux but with the known constant TEXTOR pumping system efficiency. The accuracy of this method is based on the calibration of the pressure measurement of TEXTOR which is at about ±10%. The solid line without markers represents the ideal behaviour of the flux, based on Eq. (4). The measured flux (solid line with markers) follows this behaviour with a reduced flux level of about 60%. At the operating pressure of $p_0 = 70$ bar the flux is $\phi_{TEX} = n_0 \cdot \overline{v} \cdot A_p \approx 1.7 \times 10^{17}\ \mathrm{s}^{-1}$, with a local particle density of $n_0 \approx 1.5 \times 10^{18}\ \mathrm{m}^{-3}$, and a beam flux density of $\Phi = \phi_{TEX}/A_p \approx 2.6 \times 10^{21}\ \mathrm{m}^{-2}\,\mathrm{s}^{-1}$. The scattering and deviation from the linearity are based on an unspecified external noise which appeared during the measurements. The error bars contain this noise.

The two cases shown are made using two different pumping efficiencies (100% and 70% of S_{TP}) or different background pressures, respectively. No significant difference can be seen in the behaviour of these two curves. This is due to the effective shielding of the supersonic flow by the "Zone of Silence" (see Sec. III A). The supersonic properties, measured with the help of a time-of-flight method, have been investigated in a comparable setup in the laboratory[8] showing Mach numbers up to 26 at a reservoir pressure of 20 bar.

For the injection system installed at TEXTOR this method cannot be applied. As simple proof that the generated beam has supersonic properties, the direct trajectory of gas leaving the nozzle and entering the skimmer opening has been blocked by a small plate. This modification represents the simulation of a purely effusive source. Assuming that the generated beam is not supersonic, the particle flux should not deviate strongly between the blocked and unblocked case. This is not the case however, as the thermal particle flux is a factor of 10 below the unblocked flux.

This method can provide additional information about the local background pressure, which is needed to calculate the beam properties, especially the Mach disc distance in Eq. (3).

The flux of thermalised gas ϕ_{th} through the skimmer is defined by the local background pressure surrounding the Mach cell, and can be calculated for a simple circular orifice represented by the skimmer opening by $\phi_{th} = n_{th} \cdot v_{th} \cdot A_S/4$.[13] Hence, the local background pressure at the skimmer for the highest reservoir pressure case of 70 bar ($\phi_{th} \approx 2.3 \times 10^{16}\ \mathrm{s}^{-1}$) is at about $p_b \approx 7.8 \times 10^{-2}$ mbar. The mach plane can now be calculated applying Eq. (3) and is placed at $x_M = 26$ mm. This implies that the choice of $x_{NS} = 10$ mm is too close to the nozzle concerning the Campargue[20] criterion and a strong influence by the high density at the skimmer is expectable. This can be seen as the main reason for the deviation between the measured flux and the ideal case. It also explains the negligible deviation between the fluxes for the two different background gas pressure modes ($S < S_{max}$ and $S > S_{max}$) in Figure 10 for the solid lines. No background gas can penetrate into this high density region. However, the particle flux does not follow the expected exponential behaviour according Beijerinck[21] or Beer's law, and shows a linear behaviour.

The reduction of particle fluxes can be explained by interaction of the beam particles with the outer skimmer structure, the leading edge of the skimmer and the inner structure. While in the first two cases the beam intensity would drop significantly, the latter case would cause a significant change on the beam divergence without a strong influence on the total flux. The latter is consistent with the observation in the present setup.

C. Electron density and temperature camera measurements

Figure 11 shows the beam penetration into a standard neutral beam heated plasma pulse in TEXTOR. Depending on the density and temperature, the penetration depths can vary between 20 and 80 mm in the boundary plasma of TEXTOR. The grainy impression is caused by the image intensifier, which was operating in a high gain mode in this particular plasma pulse. This statistical noise is used to deduce the error bars in Figure 11 and is also present in

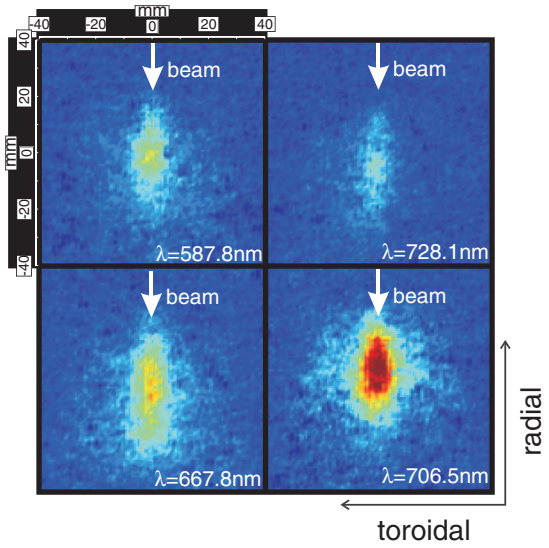

FIG. 11. Typical beam emission profiles for various spectral helium lines created by helium injections into a TEXTOR plasma. The varying emission profiles are used to deduce electron density and temperature in radial direction.

Figure 9(a). The systematic error of the line-ratio technique presented in Sec. II is not included in this error bar. Radial electron density and electron temperature profiles are extracted from the data presented in Figure 11 after a background subtraction and a toroidal integration.

In Figure 12, a comparison is shown between the established helium beam measurement at the low field side of TEXTOR[1,7,10,25] and the slow acquisition system of the new supersonic helium beam during an ohmic plasma pulse. The data is in good agreement within the error bars and with respect to the different locations. The supersonic helium beam provides n_e-T_e profiles on top of the machine and therefore has become an essential part of the plasma edge diagnostics at TEXTOR.

D. Performance of the photomultiplier system

The previous assumption in Sec. II has shown the expected intensity of the beam emission. In this section the experimental validation as well as the capability of the fast observation system are discussed.

As an example, data acquired during the flattop phase of a standard neutral beam heated TEXTOR plasma pulse #98335 ($I_p = 300$ kA, $B_t = 2.25$ T, $\bar{n}_e = 2 \times 10^{19}$ m^{-3}) has been used.

A simple method has been developed by Bencze[26] to determine the photon flux of PMT measured signals. In this case the photon noise of the detected photons is the dominating noise source.[27] The amplifier noise can be neglected.

The relative scatter $\sigma(\langle U\rangle)/\langle U\rangle$ of the measured signal voltage $\langle U\rangle$ is shown in a double logarithmic plot (see Figure 13) as a function of the signal smooth length Δt. In this plot, the signal of a stable ideal light source with a given photon flux would appear as a straight line (e.g., a photon flux of 10^7s^{-1} would lead to a measured noise equivalent on a PMT ($\eta = 1$) of $\sigma = \sqrt{I} = \sqrt{100}$ photoelectrons in a time window of $\Delta t = 10^{-5}$ s, and therefore the relative scatter would be $\sigma/I = 0.1$, etc.). In Figure 13 various photon fluxes are plotted in the range of $10^5 - 10^8$/s (dashed lines). In the measured signal (solid line) at the shortest time scales the photon noise dominates the fluctuation amplitude. Therefore, the curve relative to the dashed lines represent the actual photon flux. In the shown case the photon flux accounts for $N_{El} = 1.6 \times 10^7$ s^{-1} (dotted line). Furthermore, this plot can be used to find characteristic time scales in the signal. Though the plasma fluctuation amplitude is close to the photon noise level, time averaging methods, e.g., correlation techniques, can still be used to deduce the characteristics of this fluctuation. The

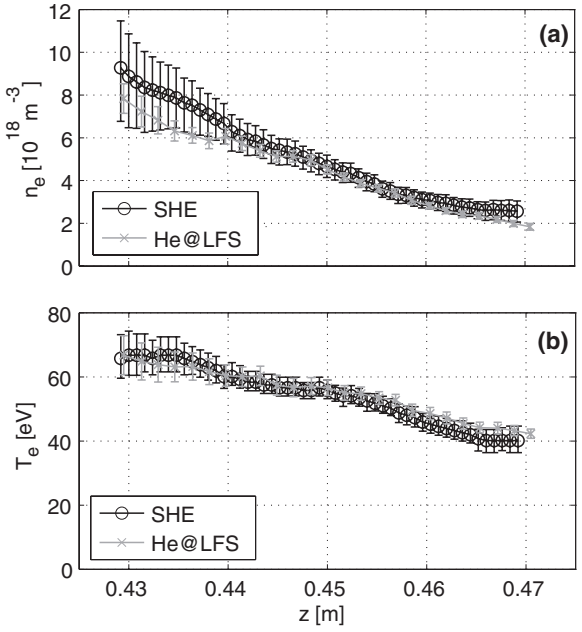

FIG. 12. Radial profiles of electron density (a) and temperature (b) profiles of discharge #105293 (averaged over $t = 2.1202-2.2412$ s) of the SHE diagnostic (black ○), and a standard He diagnostic (grey, ×).

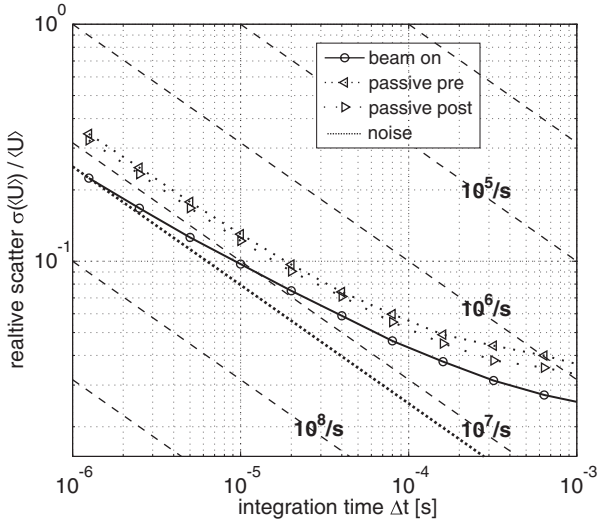

FIG. 13. Root mean square relative scatter $\sigma(\langle U\rangle)/\langle U\rangle$ of the He-beam line emission 728.1 nm (solid line, ○) as a function of the integration time for the plasma pulse #98335 (1.5702–1.6911 s, $z = 0.456$ m). Additionally $\sigma(\langle U\rangle)/\langle U\rangle$ is shown for passive background signals before and after the active beam phase (dotted lines, ▷/◁). Dashed lines indicate $\sigma(\langle U\rangle)/\langle U\rangle$ of poisson noise of constant photon flux.

resolution of single events requires a higher signal to noise ratio, e.g., a detection limit may be defined at signals 3 times higher than the actual noise level. The measured photon flux compared to the theoretical expectation in Sec. II shows a discrepancy of a factor of approximately 12, with a resulting noise level of 8% instead of an estimated 2%. There could be various reasons for this finding: (1) The assumed neutral particle density is not taking ionisation losses into account, which can be in the range of a factor 2–3 for the observed position. (2) Following plasma operation, a coating on the vacuum window surface was found absorbing 50% of the passing light. The transmission has been assumed to be ideally 4% per optical surface which may vary with the optical quality and dust. (3) An adjustment error leads to further losses of 50% as the helium beam was partially outside the observation volume.

E. Electron density and temperature fluctuations

High frequency electron density fluctuations in the edge of the TEXTOR plasma were experimentally observed in the range of 10% with various diagnostic techniques, reaching 50%–100% relative fluctuation amplitudes in the scrape-off layer region.[2,28,29] Measuring simultaneously the three spectral lines, the electron density and temperature time traces are constructed on the same time basis using the line ratio techniques described in Chap. II. The turbulent structures are characterised using these calculated time traces. As shown above, the measured photon flux limits the resolution of the recent setup to 8% in the 100 kHz range. The line ratio techniques will not effect the temporal properties of the signal but will increase the white noise level within a factor of two. Although with this noise level the resolution of single events with comparable amplitudes are not possible, the statistical parameters of the underlying turbulent structures can still be characterised using advanced data analysis methods. The auto-correlation technique has been used to deduce relative fluctuation amplitudes for electron densities and temperature signals. The white noise peak at $\tau = 0$ is removed using a linear extrapolation of the neighboring points. The resulting corrected auto-correlation peak is then used to calculate the relative fluctuation amplitude.[30] The relative fluctuation amplitude measured during the TEXTOR pulse #98335 at the nominal last closed flux surface (LCFS) is 13% for n_e-fluctuations and 7% for T_e-fluctuations. These fluctuation amplitudes are within the range of corresponding fluctuation amplitudes in the plasma edge reported in literature.[11,12] Furthermore, the auto-correlation function width can be used to determine the average de-correlation time of the turbulent structures as shown in Figure 14 (at $z = 0.456$ m). Calculating the cross-correlation function between signals of spatially distributed observation volumes, the radial size (spatial de-correlation scale) can also be determined. 2D cross-correlation functions have been calculated for n_e and T_e-fluctuations (Figure 14), and the resolved structures show similar spatial and temporal properties. The plotted contour line (dashed), indicates the correlation function level of 1/e. The tilting of the 2D correlation function in the temporal spatial plane can indicate radial propagation. However, a one dimensional detection system is not able to distinguish structures tilted in the poloidal plane from structures which are moving in radial direction only.

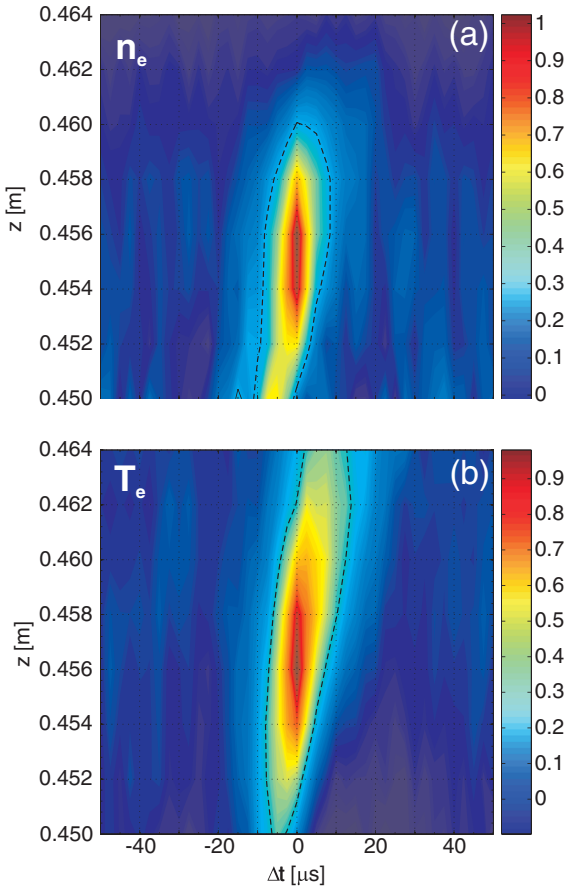

FIG. 14. Cross-Covariance Φ_N of n_e (a) and T_e (b) during pulse #98335, $t = (1.5702–1.6911)$ s with the contour $\Phi_N = 1/e$ (black, dashed line). L_r and T_L are indicated. $z_{central} = 0.456$ m, $z_{LCFS} = 0.460$ m.

The "smearing" effect of the relaxation time (Sec. II) can be neglected due to a sufficiently high local electron density in the observed area ($n_e > 4 \times 10^{18}\,\mathrm{m}^{-3}$, $T_e \simeq 40\,\mathrm{eV}$ $\Rightarrow \tau < 1\,\mu\mathrm{s}$).

Further studies across the whole measurement spatial range and various plasma conditions are necessary.

VI. CONCLUSION AND OUTLOOK

An active spectroscopy diagnostic based on beam emission spectroscopy on helium was developed for measurements of radial electron temperature and density profiles with high temporal $\Delta t \simeq 2\,\mu$s (470 kHz) and spatial resolution (2 mm) in the plasma edge of TEXTOR. The helium beam line-ratio-technique established at TEXTOR using effusive gas injection sources can be used to investigate heat and particle fluxes. However, only a supersonic injection system is able to provide a high beam density and a low beam divergence simultaneously as requested for turbulence measurements. Both properties have been achieved by a Campargue type supersonic injection system based on a special nozzle skimmer setup. In combination with a newly developed piezo valve for operation in a high magnetic field environment and using the "volume pump effect," a modulated helium beam (pulse

duration 120 ms, duty cycle 1/3) has been generated with a particle beam density of $n_0 = 1.5 \cdot 10^{18}\,\mathrm{m}^{-3}$ at a low divergence $\pm 1^\circ$ (beam width in observation volume ~9 mm).

This new injection system was designed and brought into operation at TEXTOR in combination with a sensitive detection system consisting of three 32 multi-channel photomultipliers and a CCD-camera. The latter is used for a relative calibration of the photomultipliers. It is equipped with an imaging light guide which enables the measurement of the three spectral helium lines ($\lambda_{3^1D\to 2^1P} = 667.8$ nm, $\lambda_{3^1S\to 2^1P} = 728.1$ nm, $\lambda_{3^3S\to 2^3P} = 706.6$ nm) necessary for the line-ratio-technique with one single CCD. The developed photomultiplier analogue electronics, including a flexible multiplexer readout, and the associated data acquisition enables measurements of helium line emissions of up to 470 kHz with a spatial radial resolution of $\Delta r = 2$ mm. An absolute comparison of the electron density and temperature profiles between the established effusive helium beam diagnostic, only capable of measurements with low time resolution, and the supersonic beam diagnostic is in good agreement within the error bars.

The unique temporal resolution of the new supersonic helium beam diagnostic was presented in the first plasma turbulence measurement applying beam emission spectroscopy and providing both electron density and temperature fluctuations data simultaneously. These fluctuations could be characterised by applying correlation techniques. They indicate that turbulent structures which underly the fluctuating plasma parameters are showing the same characteristic properties inside the last closed flux surface. These results are consistent with previous measurements of electron density turbulence performed with other diagnostics.

Another relevant application of the SHE diagnostic was the investigation of edge plasma structures during fast rotating resonant magnetic perturbations (RMP).[31] Combined analysis of toroidally and poloidally displaced fast edge diagnostics at TEXTOR, such as the reciprocating probe, reflectometry, and the accelerated lithium beam diagnostic, will lead to a better understanding of plasma edge physics. The supersonic helium beam diagnostic provides essential data for this study.

ACKNOWLEDGMENTS

This work was supported by the Research Centre Juelich (FZJ) and is part of a Ph.D. work at the Heinrich-Heine University Düsseldorf, Germany.

The authors would like to take this opportunity to express their gratitude to the mechanical engineer, Mr. Serge Musso. It is only with his professional advice and guidance that we have been able to complete this diagnostic and ensure it will remain operational for many years, like so many other diagnostics Serge has designed over the years at TEXTOR. Sadly, Serge passed away in 2006 and so was unable to witness this work fully completed. He shall never be forgotten and is greatly missed by ourselves and all our colleagues who knew him.

[1] E Hintz and B Schweer, Plasma Phys. Controlled Fusion **37**, A87 (1995).
[2] A Huber, U Samm, B Schweer, and Ph Mertens, Plasma Phys. Controlled Fusion **47**, 409 (2005).
[3] D. Andruczyk, S. Namba, B. W. James, K. Takiyama, and T. Oda, Plasma Devices and Oper. **14**, 81 (2006).
[4] T. Diez-Rojo, V. J. Herrero, I. Tanarro, F. L. Tabares, and D. Tafalla, Rev. Sci. Instrum. **68**, 1423 (1997).
[5] A. Hidalgo, D. Tafalla, B. Branas, and F. L. Tabares, Rev. Sci. Instrum. **75**, 3478 (2004).
[6] O. Schmitz, I. L. Beigman, L. A. Vainshtein, B. Schweer, M. Kantor, A. Pospieszczyk, Y. Xu, M. Krychowiak, M. Lehnen, U. Samm, B. Unterberg, and TEXTOR team, Plasma Phys. Controlled Fusion **50**, 115004 (2008).
[7] B. Schweer, M. Brix, and M. Lehnen, J. Nucl. Mater. **266–293**, 673 (1999).
[8] M. Brix, *Messung von Elektronentemperatur und -dichte mittels Heliumstrahldiagnostik im Randschichtplasma eines Tokamaks*, Vol. Jül-3638 (FZJ, 1998).
[9] S Brezinsek, A Huber, S Jachmich, A Pospieszczyk, B Schweer, and G Sergienko, Fusion Sci. Technol. **47**, 209 (2005).
[10] B. Schweer, Trans. Fusion Sci. Technol. **49**, 404 (2006).
[11] A. J. Wootton, B. A. Carreras, H. Matsumoto, K. McGuire, W. A. Peebles, Ch. P. Ritz, P. W. Terry, and S. J. Zweben, Phys. Fluids B: Plasma Phys. **2**, 2879 (1990).
[12] C. Hidalgo, Plasma Phys. Controlled Fusion **37**, A53 (1995).
[13] M. Wutz, H. Adam, and W. Walcher, *Theorie und Praxis der Vakuumtechnik*, Vol. 4. Auflage (Vieweg-Verlag, Braunschweig, 1988).
[14] D. R. Miller, in *Atomic and Molecular Beam Methods*, edited by G. Scoles (Oxford University Press, 1988), Vol. 1, pp. 397–405.
[15] H. Pauly, *Atom, Molecule and Cluster Beams I*, ISBN 3-540-66945-0 (Springer Verlag, 2000).
[16] J. B. Anderson and J. B. Fenn, Phys. Fluids **94**, 780 (1965).
[17] U. Bossel, F. C. Hurlbut, and F. S. Sherman, in *Rarefied Gas Dynamics*, edited by L. Trilling (Academic, New York, 1969), Vol. II, pp. 945–996.
[18] H. Ashkenas and F. S. Sherman, in *Rarefied Gas Dynamics*, edited by J. de Leeuw (Academic, New York, 1966), Vol. 2, pp. 84–105.
[19] R. Campargue, in *Rarefied Gas Dynamics*, edited by J. de Leeuw (Academic, New York, 1966), Vol. 2, pp. 279–298.
[20] R. Campargue, J. Phys. Chem. **88**, 4466 (1984).
[21] H. C. W. Beijerinck and R. J. F. van Gerwen, Chem. Phys. **96**, 153 (1985).
[22] K. Bier, *Zur Wirkung von Verdichtungsstößen im Übergangsbereich zwischen gasdynamischer und molekularer Strömungsform*, Vol. 2 (Akademie Verlag, Berlin, 1963).
[23] U. Kruezi, *Entwicklung einer Heliumstrahldiagnostik zur Messung der Elektronendichte und -temperatur mit hoher räumlicher und zeitlicher Auflösung* Vol. 62 (FZJ, 2007), ISBN 978-3-89336-476-3.
[24] O. Neubauer, G. Czymek, B. Giesen, P. W. Hütteman, M. Sauer, W. Schalt, and J. Schruff, Fusion Sci. Technol. **47**, 76 (2005).
[25] O. Schmitz, S. Brezinsek, I. Classen, M. Clever, J. W. Coenen, E. Delabie, K. H. Finken, M. W. Jakubowski, M. Kantor, A. Krämer-Flecken, U. Kruezi, M. Lehnen, Y. Liang, D. Reiter, U. Samm, B. Schweer, G. W. Spakman, H. Stoschus, G. Telesca, B. Unterberg, E. Uzgel, Y. Xu, and TEXTOR team, AIP Conf. Proc. **993**, 135 (2008).
[26] A. Bencze and S. Zoletnik, Phys. Plasmas **12**, 052323 (2005).
[27] D. Dunai, S. Zoletnik, J. Sárközi, and A. R. Field, Rev. Sci. Instrum. **81**, 103503 (2010).
[28] H. Xu, Plasma Phys. Controlled Fusion **47**, 1841 (2005).
[29] D. Dunai and S. Zoletnik, *in Proceedings of 36th EPS Conference on Plasma Physics, Sofia, 2009*.
[30] J. S. Bendath and A. G. Persol (Wilsey-Interscience, 1971).
[31] H. Stoschus, O. Schmitz, H. Frerichs, M. W. Jakubowski, B. Unterberg, S. S. Abdullaev, M. Clever, J. W. Coenen, U. Kruezi, D. Schega, U. Samm, and TEXTOR Research Team, Phys. Plasmas **17**, 060702 (2010).